Paper No.
C2025-00472

AMPP ANNUAL CONFERENCE + EXPO
APRIL 6-10, 2025 | NASHVILLE, TENNESSEE

Impact of Souring on $FeCO_3$ Corrosion Products

Adam Cutright, David Young, Bruce Brown
Institute for Corrosion & Multiphase Technology
Department of Chemical & Biomolecular Engineering, Ohio University
342 West State Street
Athens, OH 45701
United States

Abstract

Simulation of reservoir souring has been a heretofore neglected area of corrosion research. The procedure followed herein involves forming a sweet corrosion product layer, addition of 100ppm of H_2S, and allowing the system to continue to evolve. The experimental apparatus used was a 2L glass cell with 5 X65 steel specimens evenly spaced, which allowed for *in situ* corrosion rate monitoring and extraction of specimens for surface analysis. When the $FeCO_3$ was challenged with H_2S, the general corrosion rate remained the same. FeS was detected on the samples, but no significant change was observed in the $FeCO_3$. However, there was a significant change in the open circuit potential (OCP) immediately following the addition of H_2S to the system.

Key words: Corrosion mechanisms, Corrosion rate, Hydrogen sulfide, Oil and gas, Carbon dioxide

Introduction

In the oil and gas industry, souring is the phenomenon in which H_2S appears in a reservoir previously containing no detectable H_2S. This work aims to focus on corrosion issues that initiate during the early onset of souring. The assumption is that prior to souring the dominant corrosive gas species will be CO_2. To appropriately replicate the environment a pipeline might experience when undergoing souring, two important questions must be answered. What concentrations of H_2S are present when souring begins to occur? What is the timescale of the souring process? In Figure 1, shown below, is an example where the H_2S concentration vs time was measured over 25 days in two separate reservoirs.[1]

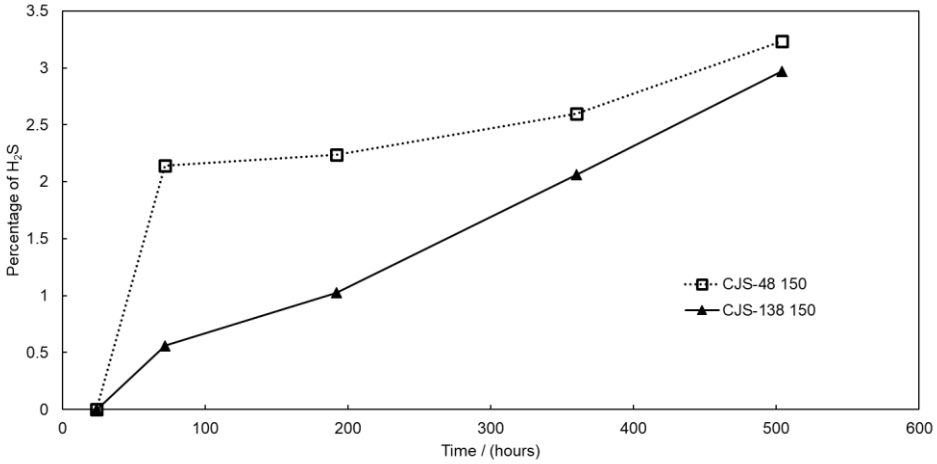

Figure 1. H_2S concentration over time in a souring reservoir where the two lines represent different sampled produced oils.[1]

Here it can be seen that, in the above case, the concentration of H_2S starts at zero and then progressively increases over time to higher and higher values.

It can be assumed that at the onset of souring the concentration of H_2S can be extremely low, and this low concentration could persist for a significant period of time. Therefore, this work is centered on introducing small concentrations of H_2S to existing sweet systems which have had sufficient time to develop corrosion product layers and maintaining the concentration of H_2S at these low levels. The specimens are then analyzed to investigate any impact the H_2S has had on the existing layer, as well as any initiation of localized corrosion.

In certain corrosive environments, after the metal has begun to corrode, what is known as a corrosion product layer can begin to form. The exact nature of the layer is largely dependent on environmental parameters such as temperature and pH, as well as the corrosive gases present. The two of particular interest to this work are iron carbonate ($FeCO_3$) and iron sulfide (FeS). Iron carbonate is formed in CO_2 environments and can be protective, an example of such an iron carbonate can be seen in Figure 2. An accompanying corrosion rate plot, shown in Figure 3, shows the decrease in the general corrosion rate associated with the formation of this protective layer.

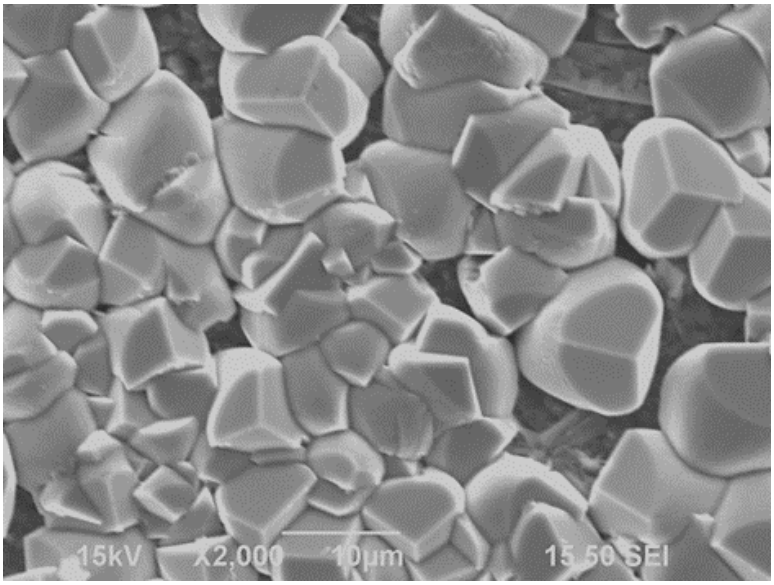

Figure 2. Protective iron carbonate layer.[2]

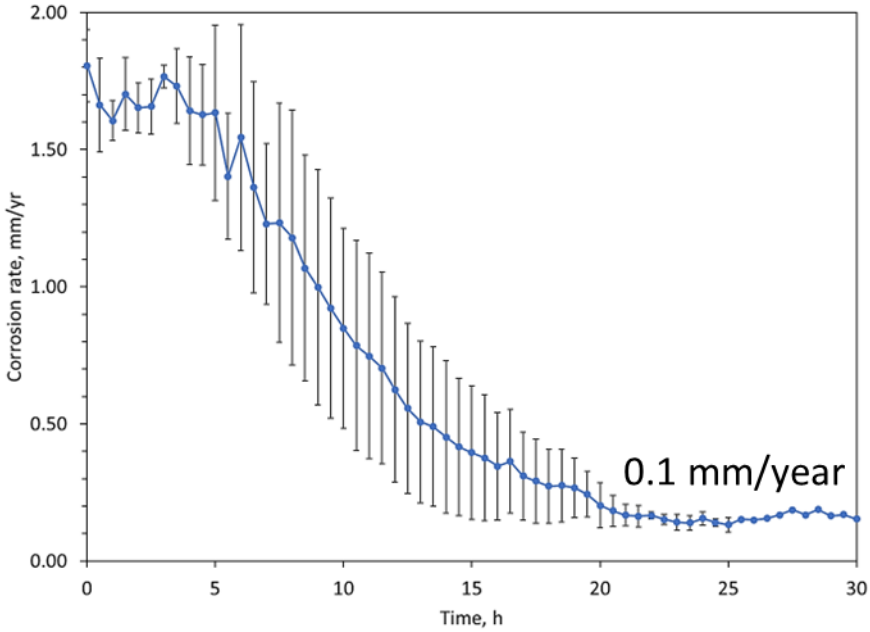

Figure 3. Corrosion rate over time during the formation of iron carbonate at 80 °C and pH 6.6, $S_{initial}(FeCO_3) = 150$.[2]

In systems containing H_2S it is more common to find an iron sulfide layer, an example of which can be seen in Figure 4. These layers can also provide a retardation in the general corrosion rate, as is demonstrated by the plot in Figure 5, but the degree of protection against localized corrosion provided by an iron sulfide layer is questionable.

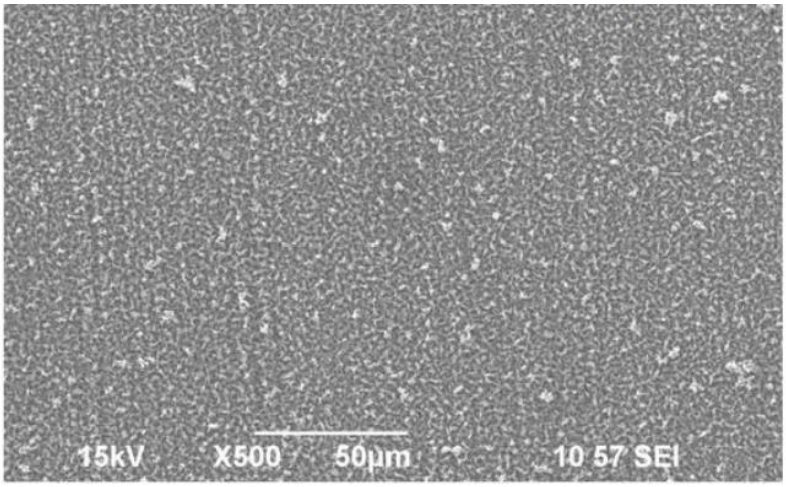

Figure 4. Iron sulfide layer.[3]

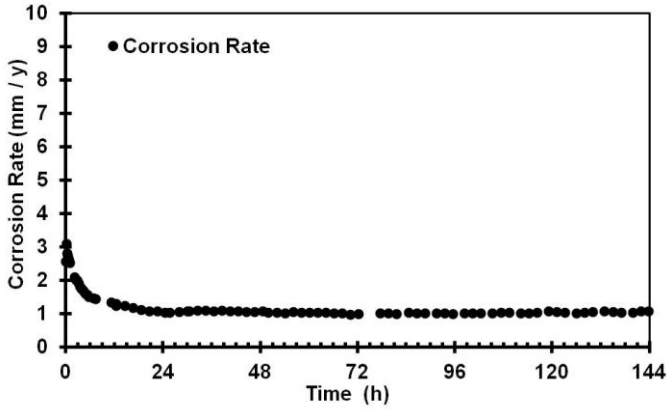

Figure 5. Corrosion rate vs. time in 10% H_2S/N_2 at 80 °C, pH 6.0.[4]

Experimental Procedure

Equipment

- Impeller
- Gamry Reference 600 Potentiostat
- 1 wt.% NaCl electrolyte
- H_2S/CO_2 mixed gas
- CO_2 gas
- Gastec pump and detector tubes
- X65 metal samples
- pH probe
- Thermocouple

Test Apparatus

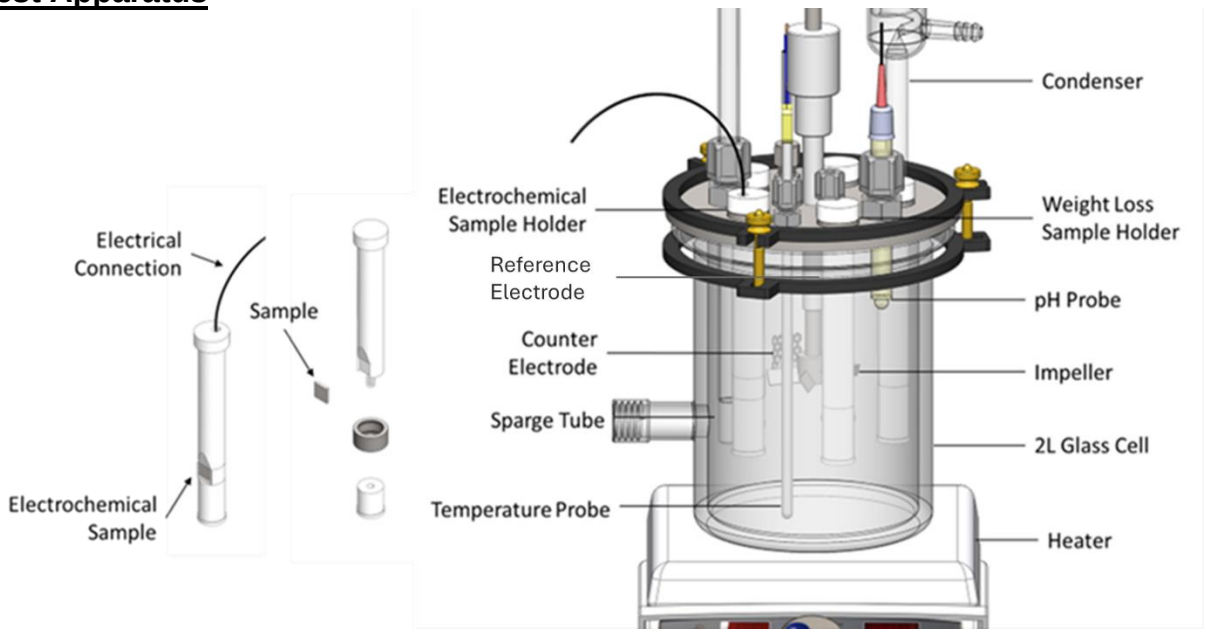

Figure 6. Glass cell setup and sample holders used during experimentation.

Material Tested

X65 Steel – uniform, fine structure of pearlite in a ferrite matrix.

Table 1. X65 steel composition

C	Mn	Nb	Ti	V	Mo	Cu	Cr	Ni	Fe
0.05%	1.40%	0.04%	0.01%	0.03%	0.07%	0.11%	0.23%	0.24%	Bal

Test Matrix

Parameter	**Addition of H_2S**
Temperature	**80°C**
pCO_2	**0.53 bar**
Solution	**1 wt.% NaCl**
Specimen	**X65 Steel**
Flow	**Quiescent**
Initial pH	**6.60 ± 0.10**
H_2S concentration added	**100 ppm**

Procedure

The general procedure for these experiments can be broken down into two sections, preparation for the experiment and the experiment itself. In terms of preparation required, the cell is cleaned and assembled as is shown in Figure 6. The cell is then sparged with pure CO_2 for at least 2 hours prior to the introduction of metal samples to purge all O_2 from the cell as well as facilitate electrolyte CO_2 saturation. The cell is then heated to the desired temperature and the pH adjusted using either deoxygenated hydrochloric acid or sodium bicarbonate solution as needed. The metal specimens, whose composition is reported in Table 1, are polished starting at 180 grit abrasive paper and moving up to 600 grit paper, as well as being sonicated in isopropyl alcohol; to confer a clean and uniform surface on all samples at the start of the experiment. The specimens are then inserted into the cell and the experiment begins.

The electrochemical testing consists of open circuit potential (OCP), linear polarization resistance (LPR), electrochemical impedance spectroscopy (EIS), and potentiodynamic sweep measurements. The OCP, LPR, and EIS measurements are performed periodically over the duration of the experiment to give continuous information about the corrosion occurring in the cell, while the potentiodynamic sweeps are only performed at the end of the experiment. Potentiodynamic sweeps were taken as two distinct separate scans: first from OCP to more negative potentials to obtain the cathodic sweep, then after allowing the sample to return to OCP, the last scan was from OCP to more positive potentials to obtain the anodic sweep. The results shown are the combination of these two scans. The LPR and EIS data can be used to determine the corrosion rate, while the potentiodynamic sweeps can give insight into any mechanistic changes occurring in the electrochemical reactions on the metal surface.

The experiments performed which are presented in this paper involve the formation of an iron carbonate layer in pure CO_2 conditions. After iron carbonate layer formation, specimens are removed from the cell for surface analysis and a concentration of H_2S is added to the gas stream. The experiment continues for a period of time during which specimens may be extracted to characterize the development of the corrosion product layer. Samples are also extracted once the experiments are concluded.

Results

The formation of iron carbonate in these experiments occurs at a temperature of 80 °C and a pH of 6.6, as the initial procedure for this type of iron carbonate layer formation was adapted from research by other researchers at the ICMT.[2] The saturation value with respect to iron carbonate, $S(FeCO_3)$, as calculated by the equation developed by Ma[5], is typically less than 30-40 during the formation period, which lasts around 10 days. A typical example of the formation of iron carbonate can be seen in Figure 7.

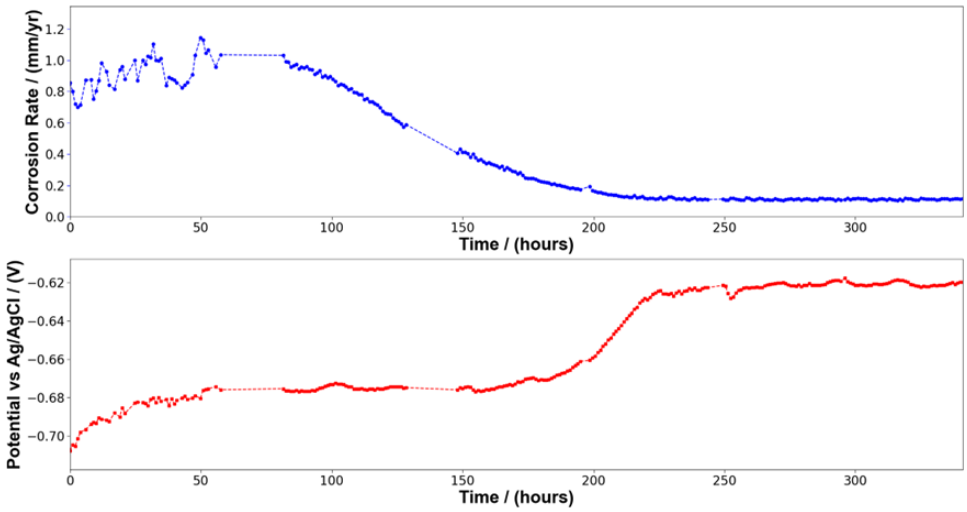

Figure 7. Corrosion rate and open circuit potential vs. time during the formation of iron carbonate.

From Figure 7 it can be seen that the corrosion rate decreases to ~0.1 mm/year over the course of 10 days, with a corresponding increase in the OCP of ~80 mV; both of which are typical of the formation of a protective iron carbonate layer.[6] The iron carbonate layer that is typically formed under these conditions can be seen below in Figure 8 and Figure 9. The layer consists of two parts, the inner layer which is dense and can contain a higher concentration of residual alloying elements left behind after the corrosion has occurred, and the outer layer which appears as large crystals adhering on top of the inner layer.

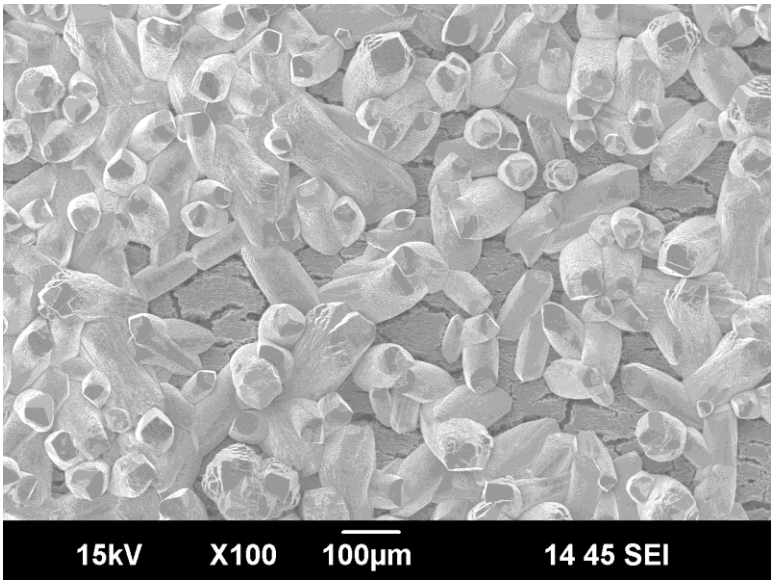

Figure 8. SEM image of iron carbonate.

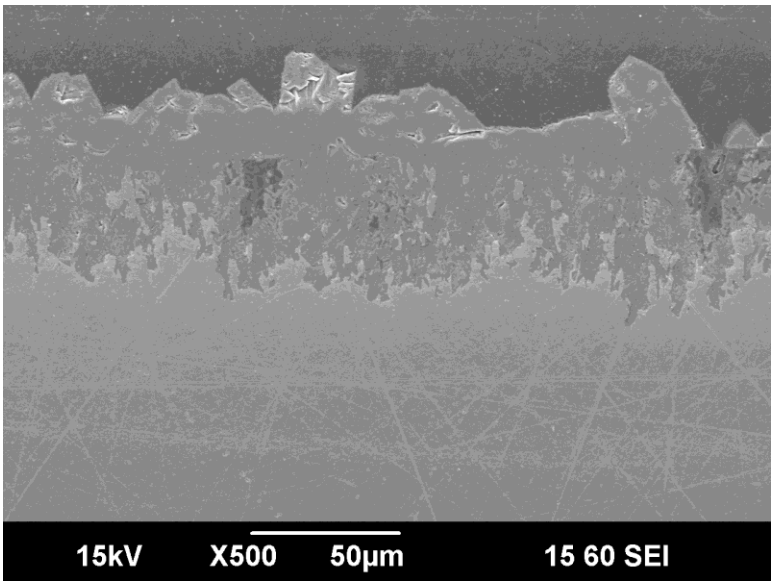

Figure 9. Cross-section SEM image of iron carbonate.

Figure 10 below shows the corrosion rate and OCP vs. time for an experiment involving the formation of iron carbonate over a period of ~10 days followed by the addition of 100 ppm H_2S. During the formation process, the corrosion rate decreased to ~0.1 mm/year, and the OCP increased by ~70 mV as had been previously observed in the formation of a protective iron carbonate layer.

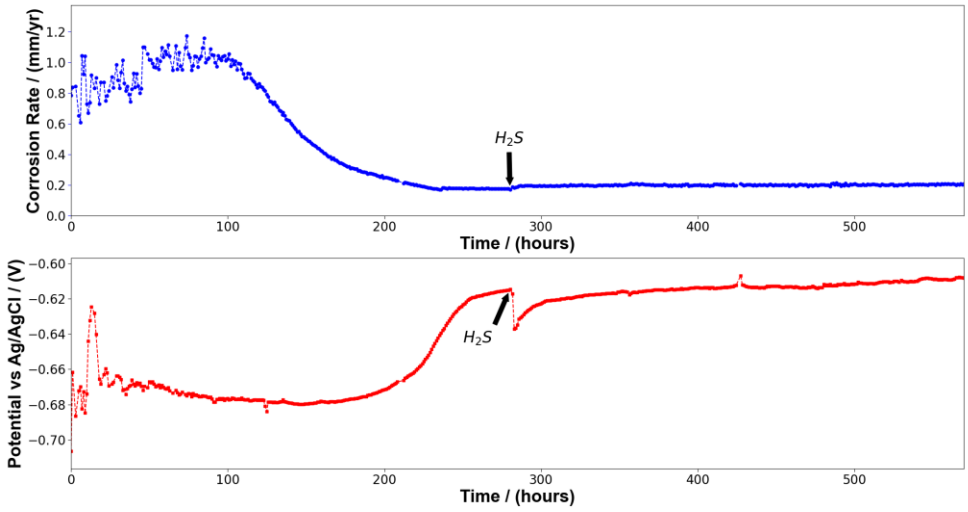

Figure 10. Corrosion rate and OCP vs time during formation of iron carbonate and subsequent addition of 100 ppm H_2S.

Following the addition of the H_2S, there was a negligible change in the general corrosion rate, however, there was an immediate decrease in the OCP. This change in the OCP was slowly reversed over the course of roughly 2 days, at which point it held to a

consistent value. SEM analysis following the addition of the H_2S showed no noticeable change in the layer at both 8- and 12-day exposures as can be seen in Figure 11 and Figure 12 below. Both the inner and outer layer of iron carbonate appear intact and essentially unchanged following the exposure to H_2S.

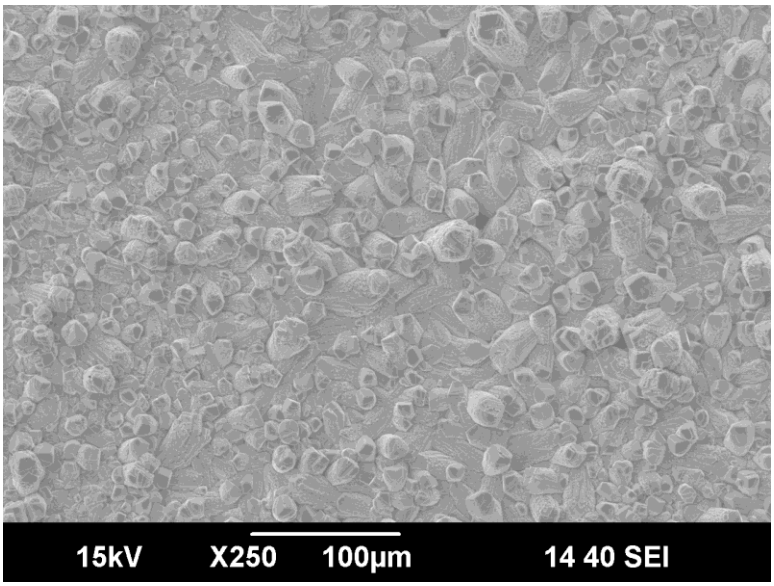

Figure 11. SEM image of the iron carbonate layer after 8-days of exposure to 100 ppm H_2S.

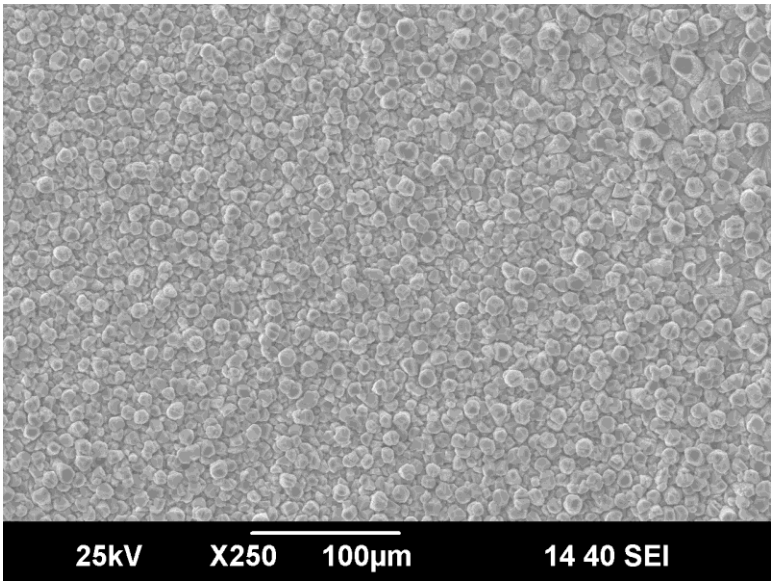

Figure 12. SEM image of the iron carbonate layer after 12-days of exposure to 100 ppm H_2S.

Raman analysis of the samples indicated the presence of both iron carbonate and iron sulfide as expected, which can be seen in Figure 13 below.

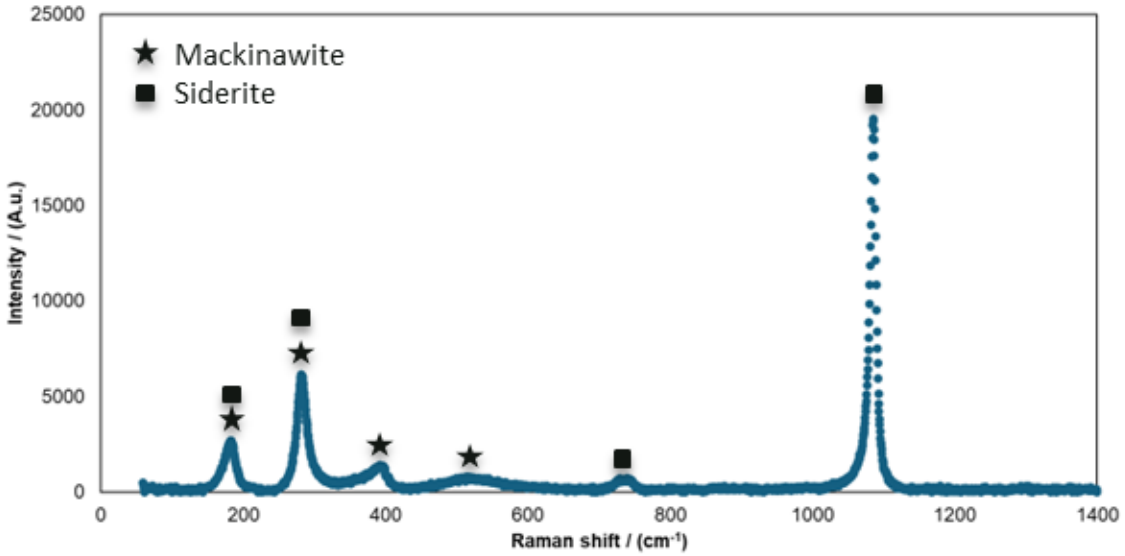

Figure 13. Raman spectroscopy of sample containing iron carbonate exposed to 100 ppm H_2S for 12 days with analysis from RRUFF.info website.[7]

Figure 14 shows the corrosion rate and OCP vs. time for an experiment where the apparent formation time of the iron carbonate layer was significantly shorter than in previous experiments, with the corrosion rate dropping to 0.1 mm/year in ~4 days, and the increase in the OCP occurring over the same duration. The experiment continued until the total time allowed for formation was similar to previous experiments, ~10 days, before H_2S was added to the system. Based on the electrochemical data shown in Figure 14, which shows the corrosion rate decreasing to ~0.1 mm/year and the OCP increasing by ~70 mV it was assumed that a fully protective iron carbonate layer had been successfully formed on the metal surface.

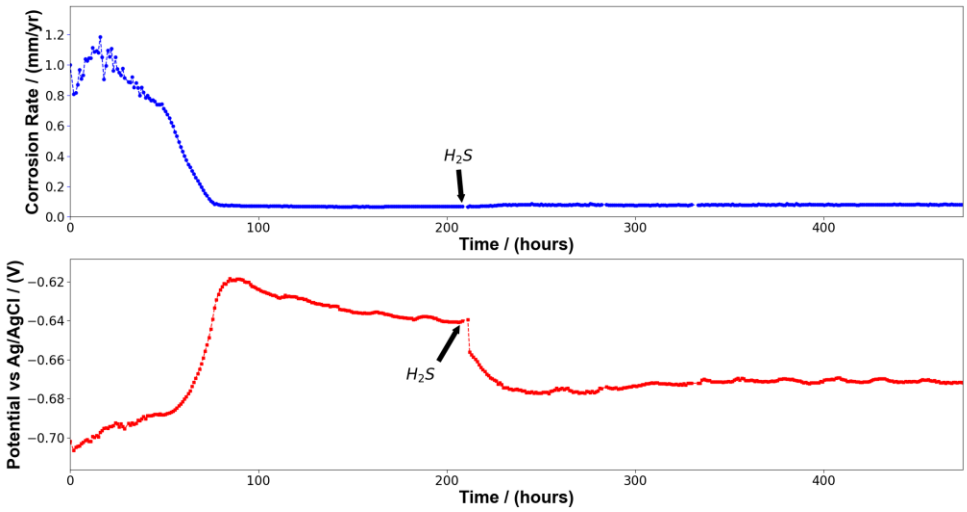

Figure 14. Corrosion rate and OCP vs. time during formation of the iron carbonate layer and subsequent addition of 100 ppm H_2S.

Upon the addition of the 100 ppm of H_2S to the system the corrosion rate remained constant, but the same decrease in the OCP that had been observed previously was observed again. However, unlike in previous experiments after the decrease in the OCP, the OCP did not return to its previous value but instead stayed at the new value for the remainder of the experiment. The SEM image shown below in Figure 15 shows how the iron carbonate layer present appeared after 2 days of exposure to H_2S. EDS analysis shown in Figure 16 and Figure 17 indicates that sulfur species are being detected, indicating the presence of an iron sulfide.

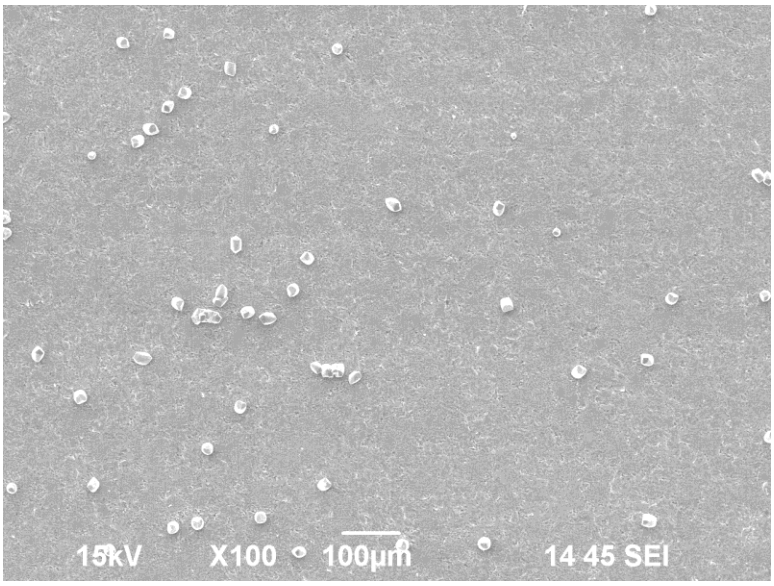

Figure 15. SEM image of iron carbonate layer after 2-day exposure to 100 ppm H_2S.

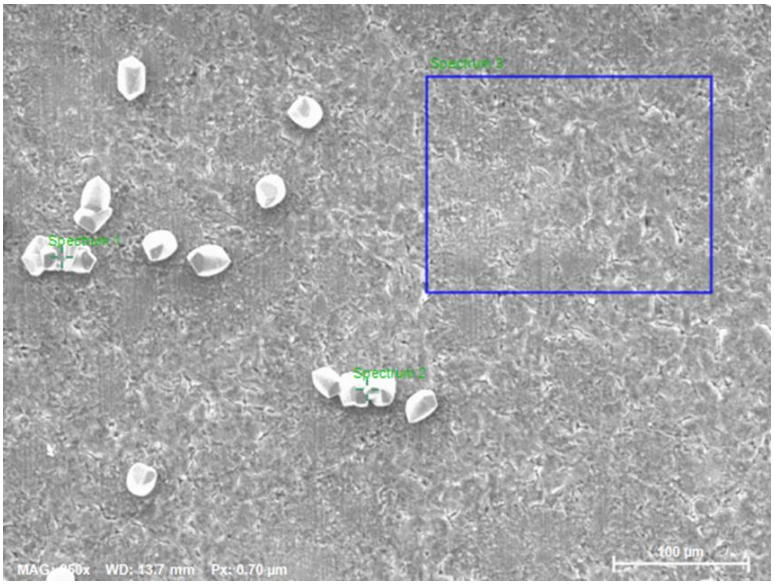

Figure 16. SEM image indicating location of EDS analysis.

Spectrum 3

Element	At. No.	Mass [%]	Mass Norm. [%]	Atom [%]	abs. error [%] (3 sigma)
Fe	26	53.48	75.12	62.02	5.55
O	8	4.04	5.68	16.37	0.36
C	6	1.27	1.78	6.84	0.15
S	16	2.28	3.20	4.60	0.22
Cr	24	3.17	4.45	3.94	0.30
Ni	28	3.30	4.64	3.65	0.40
Al	13	0.42	0.59	1.00	0.06
Tl	81	2.60	3.65	0.82	0.25
Mn	25	0.63	0.89	0.74	0.06
		71.19	**100.00**	**100.00**	

Figure 17. Results of EDS analysis on sample exposed to 100 ppm H_2S for 2 days.

Cross-section analysis, presented in Figure 18, shows that the layer which was present was very thin compared to previous experiments, having a thickness of only 5-10 µm.

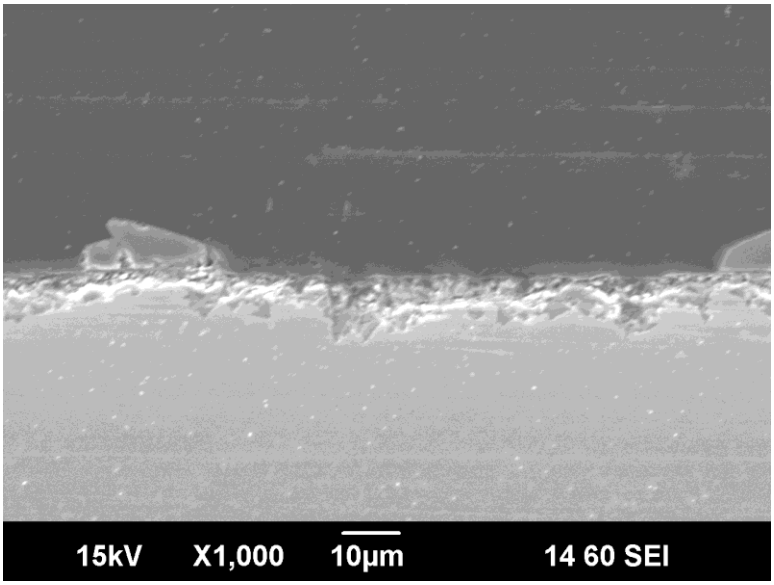

Figure 18. Cross-section SEM image of iron carbonate after 2-day exposure to 100 ppm H_2S.

Further exposure times see similar results, images taken after 7 and 11 days are shown below in Figure 19, Figure 20, and Figure 21.

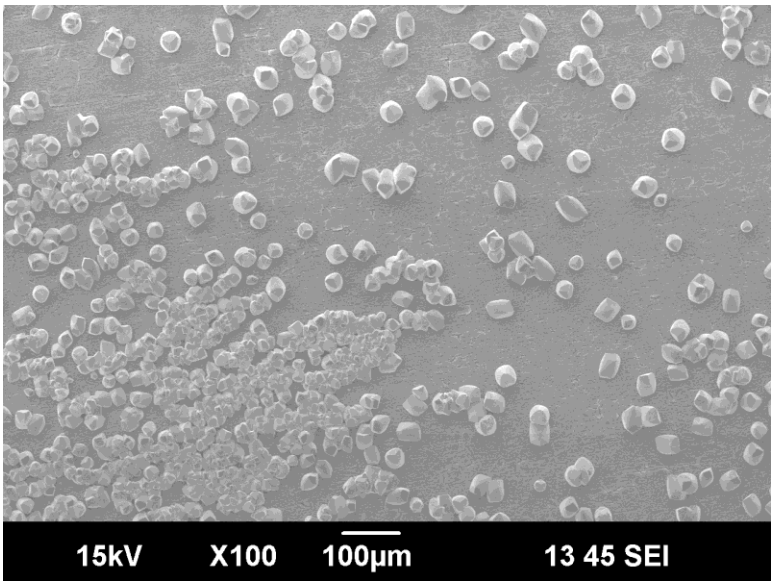

Figure 19. SEM image of iron carbonate after 7-day exposure to 100 ppm H_2S.

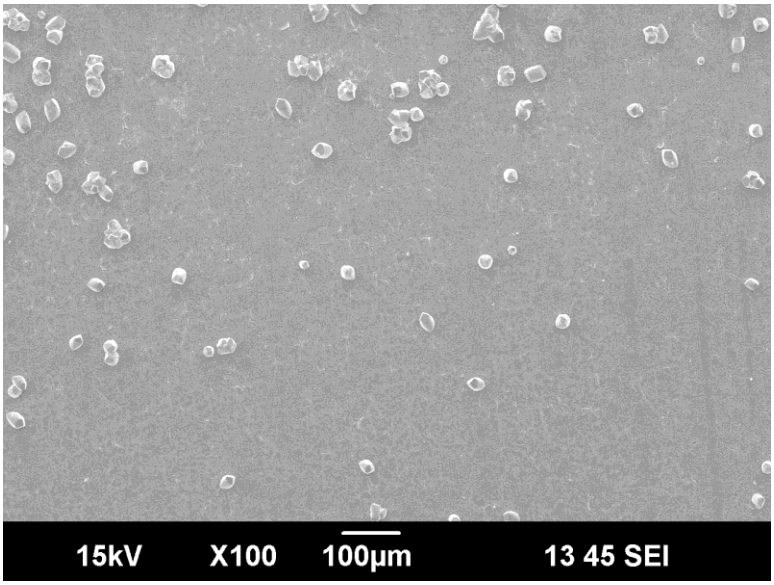

Figure 20. SEM image of iron carbonate after 11-day exposure to H_2S.

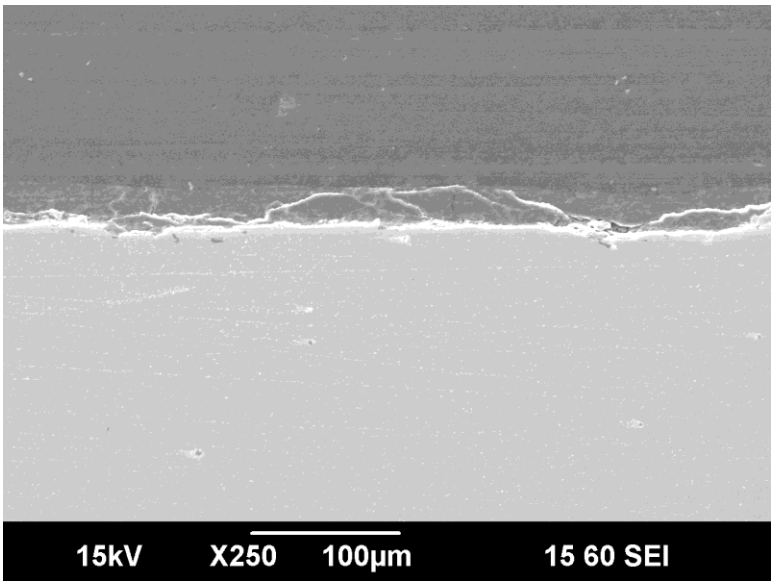

Figure 21. Cross-section SEM image of iron carbonate after 11-day exposure to 100 ppm H_2S.

As has been shown, after the addition of the H_2S, the bulk of the outer layer of iron carbonate appears to have disappeared, however, the inner layer remained intact and uniform across the sample surface at all times.

As has been stated previously, at the end of each experiment a potentiodynamic sweep is performed in order to better understand the changes that occurred over the course of the experiment. The results of these potentiodynamic sweeps are presented below in Figure 22.

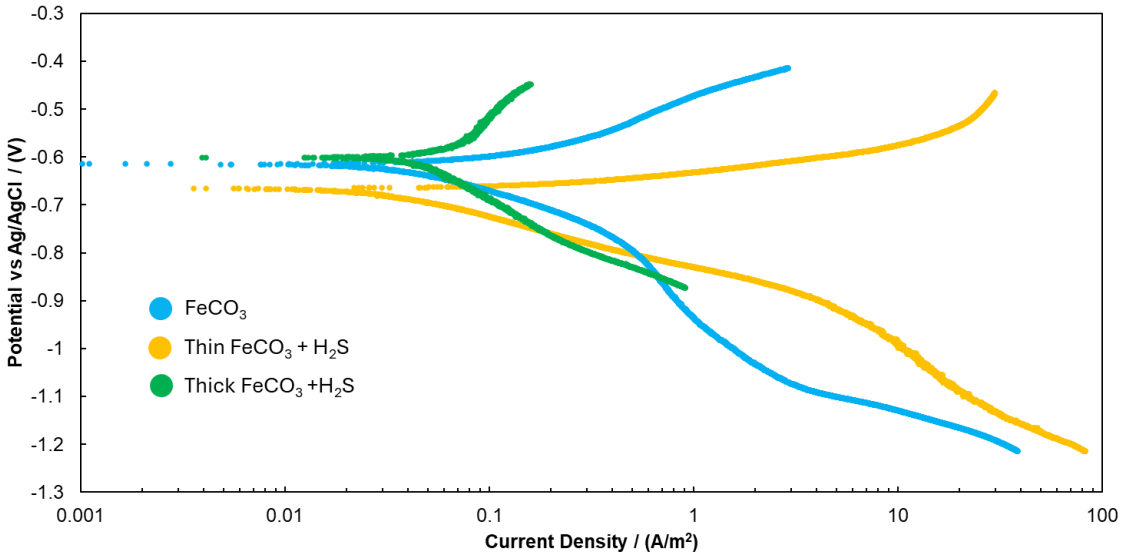

Figure 22. Potentiodynamic sweeps taken at the end of the various experiments presented previously.

From these sweeps certain observations can be made. Taking the light blue sweep, which represents the potentiodynamic sweep taken on an iron carbonate layer formed over ~10 days as a baseline, there are noticeable changes when H_2S is added. The green sweep is from an iron carbonate layer, formed over 10 days, and then subjected to 100 ppm H_2S for 12 days. It can be seen that there is a noticeable retardation in the anodic reaction, almost no change to the cathodic reaction, but there is a decrease in the mass transfer limiting current. In comparison, the orange sweep from an iron carbonate layer that was formed over 4 days and then subjected to 100 ppm H_2S for 11 days shows a noticeable decrease in the OCP, along with an acceleration of the anodic reaction, and retardation of the cathodic reaction. The mass transfer limiting current also appears to have increased. From these results it could be possible that upon exposure to H_2S, an FeS layer is being formed on and around the existing iron carbonate layer and is acting as additional surface area for the cathodic reaction to occur. However, it also appears that the thickness of the iron carbonate layer plays a role in whether this phenomenon occurs or not, with the thick layer formed over 10 days showing a different behavior than the thin layer formed over only 4 days.

Conclusions

- Iron carbonate layer formed over 10 days showed no impact from the addition of 100 ppm H_2S over the experiment duration
  - Initial change in the OCP but this returns to its original value after a few days
  - Confirmed by LPR
- Iron carbonate layer formed over 4 days shows no visible change in the layer after the addition of 100 ppm H_2S
  - There is a noticeable and permanent decrease in the OCP
  - Confirmed by potentiodynamic sweeps and LPR

References

1. Mi, J., B. Zhang, Z. Shen, W. Huang, A. Casalins, and C. Liu, *J. Nat. Gas Geosci.* 2 (2017): pp. 201–208.
2. Ayyagari, S., “Protectiveness of Corrosion Product Layers in Aqeous CO2 Environments” (Ohio University, 2022).
3. Ning, J., “Investigation of Polymorphous Iron Sulfide in H2S Corrosion of Mild Steel” (Ohio University, 2013).
4. Zheng, Y., “Electrochemical Mechanism and Model of H2S Corrosion of Carbon Steel,” Dissertation, Ohio University, 2015.
5. Ma, Z., X. Gao, B. Brown, S. Nesic, and M. Singer, *Ind. Eng. Chem. Res.* 60 (2021).
6. Han, J., S. Nešić, Y. Yang, and B. Brown, *Electrochimica Acta - ELECTROCHIM ACTA* 56 (2011): pp. 5396–5404.
7. Armbruster, T., and R.M. Danisi, eds., “Highlights in Mineralogical Crystallography” (De Gruyter (O), 2016), p. I–IV, https://doi.org/10.1515/9783110417104-fm (May 11, 2024).